

FlowDreamer: A RGB-D World Model with Flow-based Motion Representations for Robot Manipulation

Jun Guo^{*,1,2}, Xiaojian Ma^{*,#,1}, Yikai Wang^{*,3}, Min Yang^{1,4}, Huaping Liu^{#,2}, Qing Li^{#,1}

¹State Key Laboratory of General Artificial Intelligence (BIGAI)

²Department of Computer Science and Technology, Tsinghua University

³School of Artificial Intelligence, Beijing Normal University

⁴School of Artificial Intelligence and Automation, Huazhong University of Science and Technology

^{*}Equal Contribution [#]Corresponding Author

<https://sharinka0715.github.io/FlowDreamer/>

Abstract

This paper investigates training better visual world models for robot manipulation, i.e., models that can predict future visual observations by conditioning on past frames and robot actions. Specifically, we consider world models that operate on RGB-D frames (RGB-D world models). As opposed to canonical approaches that handle dynamics prediction mostly implicitly and reconcile it with visual rendering in a single model, we introduce FlowDreamer, which adopts 3D scene flow as explicit motion representations. FlowDreamer first predicts 3D scene flow from past frame and action conditions with a U-Net, and then a diffusion model will predict the future frame utilizing the scene flow. FlowDreamer is trained end-to-end despite its modularized nature. We conduct experiments on 4 different benchmarks, covering both video prediction and visual planning tasks. The results demonstrate that FlowDreamer achieves better performance compared to other baseline RGB-D world models by 7% on semantic similarity, 11% on pixel quality, and 6% on success rate in various robot manipulation domains.

1. Introduction

We study developing better visual world models for robot manipulation tasks. In robotics, a visual world model [24] needs to perform the following steps: 1) **dynamics prediction**: predict the future motion given the current sensory observations (about robot and environment states) and robot action; and 2) **visual rendering**: render the visual observations after the motion happens. A visual world model captures the underlying world dynamics and can be used as a learnable simulator to help produce and evaluate motion plans of robot manipulators in company with model-based

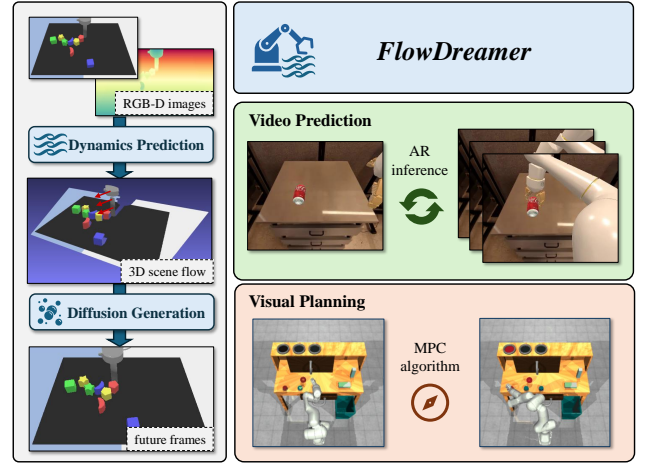


Figure 1. **Proposed RGB-D world model with flow-based motion representations.** FlowDreamer adopts a two-stage prediction framework, which explicitly predict scene flow as motion representations. FlowDreamer achieves better results on future frame prediction and visual planning tasks in various robot manipulation domains.

planning algorithms [63, 87, 94, 98]. The use of visual world models alleviates the need for precise scene modeling and simulation [14, 37], making it a promising research direction. In this paper, we specifically focus on world models that operate on RGB-D frames (RGB-D world models), which are commonly adopted sensory observations in robot manipulation tasks.

Existing visual world models have undergone rapid development in recent years. Starting from early approaches that utilize recurrent neural networks (RNNs) [18, 25–27, 29, 39], powerful diffusion-based generative models [7, 19, 32, 64, 70, 71] have gain popularity in recent world models [1, 2, 40, 59]. However, regardless of the architectures of these models, they mostly reconcile the two aforementioned steps (dynamics prediction and visual rendering)

in a single model. These design choices not only reduce the model’s transparency but also, as our later experiments show, impair its future prediction performance. We hypothesize that models trained solely with frame prediction loss tend to prioritize improving the fidelity of rendered visual appearances while placing less emphasis on accurate dynamics prediction. This highlights the importance of exploring methods that explicitly model dynamics prediction.

To this end, we propose FlowDreamer, a RGB-D world model that explicitly models dynamics prediction to enhance the predictive capability of world models. FlowDreamer adopts a two-stage framework to predict the environment dynamics and render the visual observations separately. Specifically, FlowDreamer introduces explicit modeling of 3D dynamics by leveraging 3D scene flow [82], which is a versatile representation that describes the motion of objects within a scene. In the first stage, a scene flow prediction module independently predicts the dynamic changes induced by given actions. This module is trained with a scene flow prediction loss to ensure robust supervision of the scene dynamics, thereby endowing the world model with an enhanced understanding of dynamics in 3D space. In the second stage, we employ a conditional diffusion model [32, 71] that predicts the next visual observation based on the current observation and the motion information provided by the scene flow prediction module. Despite its modularized nature, our model can be trained in an end-to-end fashion.

We validate the effectiveness of our method on multiple benchmarks commonly used in robotic manipulation. On action-conditioned benchmarks (*e.g.*, RT-1 [6], Language Table [51]), our approach achieves better visual performance comparable to normal RGB-D world models, with a 7% increase in semantic similarity and 11% on pixel quality. Evaluations on VP² visual planning benchmark [77] with RoboDesk [41] and Robosuite [99] tasks reveal a 6% increase in the success rate in manipulation tasks.

In summary, our main contributions are as follows:

1. We propose FlowDreamer, a two-stage RGB-D world model with dynamics and visual prediction module, which can be trained in an end-to-end fashion despite its modularized nature.
2. We introduce a scene flow prediction module that adopts 3D scene flow on RGB-D space as a general motion representation to supervise dynamics prediction and enhance dynamics modeling.
3. We perform comprehensive evaluations across several benchmarks, demonstrating the efficacy of our approach in both visual performance and visual planning tasks.

2. Related Work

2.1. Generative World Models in Robotics

World models [24], also known as dynamic models, refer to techniques that predict the future state based on current observations and given conditions. In robotics, control strategies can leverage the generative capability of these models for planning, learning, or reducing the cost associated with interactions in the real environment. A world model typically requires the robot’s current observation in the form of latent states, sensor measurements, or visual information as input and produces future observations while also potentially predicting higher-level information such as rewards, values, or subsequent actions.

Existing work in this domain can be broadly categorized into two types, namely *control-based* world models and *instruction-based* world models. In *control-based* world models [20, 21, 63, 87, 94, 98], the conditioning inputs are robot control signals, including joint forces or velocities, end-effector positions, or movement commands. These models can serve as simulators for the environment and facilitate approaches such as model-based reinforcement learning [18, 25–27, 39, 66, 73, 74, 88] and model predictive control [28, 29]. Many studies [2, 8, 40, 53, 54, 58, 59, 79] have also trained world models within games with players’ interaction signals as input, employing neural networks as the game engine. In contrast, *instruction-based* world models [1, 4, 16, 17, 34, 43, 47, 94, 97] take task-related instructions, *e.g.*, task identifiers or natural language descriptions, as conditions to generate a sequence of future states or actions. This approach not only envisions future world states but also simulates the execution of policies, thereby allowing inverse dynamics to derive robot control parameters from observations [4, 43] or enabling fine-tuning into a vision-language-action (VLA) model [11, 16, 17, 96]. This paper proposes a *control-based* world model that uses robot actions as conditions and employs scene flow as an intermediate representation to simulate and predict environmental dynamics, ultimately generating images that are interpretable by human observers.

2.2. Dynamics Modeling

Most existing world models are trained in an end-to-end manner with supervising signals to directly predict future states without explicitly modeling the dynamical processes. Explicit modeling of the dynamics underlying environmental state changes can enhance the interpretability of the world model and improve prediction accuracy. In the field of video generation, there are several works [22, 30, 52, 57, 69] that model the motion between frames to better control and enhance the performance of video generation models. Early works [10, 56, 91] employed SE(3) transformations as an intermediate representation of object mo-

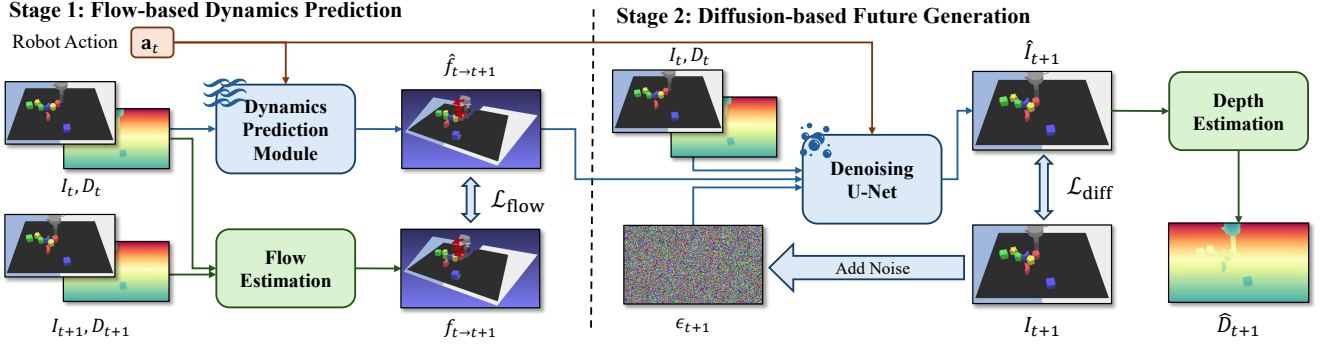


Figure 2. **Overview of FlowDreamer.** At stage 1, FlowDreamer receives the RGB-D frame and the robot action as input to explicitly predict the scene flow as motion representations. At stage 2, FlowDreamer leverages a denoising U-Net to generate high-resolution next-step future observation via diffusion.

tion. This approach is limited to rigid bodies and requires the world model to possess object-centric awareness, which requires extra segmentations of training data. An alternative representation is *flow* [43, 90], which is referred to as optical flow [33, 50] in 2D images and as scene flow [82] in 3D space. Flow is defined as the displacement of every point in the observation space from one timestep to the next, which provides a universal and flexible means to represent various forms of motion, including non-rigid objects. In order to extract flow information from the training sequences of world models, flow estimation methods are employed to compute the displacement between adjacent frames. In the 2D domain, numerous methods, including both traditional [5, 9, 33, 50] and deep learning-based [15, 35, 44, 62, 67, 68, 72, 75, 92] approaches, have been developed to estimate optical flow. In 3D space, several deep learning methods [38, 42, 48, 49, 81, 89] have shown promise in estimating scene flow, while the task remains generally more challenging. Our approach utilizes 3D scene flow in the RGB-D space as the representation of motion, which can be obtained by integrating optical flow from consecutive frames with the corresponding depth information.

3. FlowDreamer: A RGB-D World Model

In this section, we illustrate the framework of our FlowDreamer. Fig. 2 depicts the overall framework of our method. FlowDreamer is a two-stage action-conditioned RGB-D world model, which receives the current RGB-D observation (I_t, D_t) and the robot action \mathbf{a}_t as the input and predicts the future RGB observations I_{t+1} . At stage 1, we start from an RGB-D observation image and a robot action, predicting the 3D scene flow $f_{t \rightarrow t+1}$ between the current and the next frame (Sec. 3.2). At stage 2, we apply a diffusion denoising network condition on the RGB-D image (I_t, D_t) and the predicted scene flow $f_{t \rightarrow t+1}$ to generate the observation I_{t+1} at the next timestep from a random noise ϵ_{t+1} (Sec. 3.3).

3.1. Background: Latent Diffusion Models

Diffusion models [32, 70, 71] progressively transform data into noise through a forward diffusion process and then learn to reverse this process to generate high-quality samples. Latent diffusion models [64] extend this framework by performing the diffusion process in a lower-dimensional latent space rather than directly in the pixel space. By leveraging a learned encoder [80] to project data into a compact latent representation, latent diffusion models achieve significant improvements in computational efficiency and scalability while still maintaining high fidelity in the generated samples. In the forward process, small amounts of Gaussian noise are incrementally added to the data, gradually destroying its structure, which can be formatted by

$$q(\mathbf{z}^k | \mathbf{z}^{k-1}) = \mathcal{N}(\mathbf{z}^k; \sqrt{1 - \beta^k} \mathbf{z}^{k-1}, \beta^k \mathbf{I}), \quad (1)$$

where \mathbf{z}^k is the noised latent, β^k is a variance schedule controlling the noise level, both at k -th denoising step. The reverse process can be modeled by a neural network ϵ_θ which aims to progressively denoise the sample, recovering \mathbf{z}^0 from \mathbf{z}^k (which is approximately Gaussian):

$$p_\theta(\mathbf{z}^{k-1} | \mathbf{z}^k) = \mathcal{N}(\mathbf{z}^{k-1}; \mu_\theta(\mathbf{z}^k, k), \Sigma_\theta(\mathbf{z}^k, k)). \quad (2)$$

During training, we sample a timestep $t \in [1, K]$ and add a Gaussian noise $\epsilon^k \sim \mathcal{N}(0, \mathbf{I})$ to the clean sample \mathbf{z}^0 by $\mathbf{z}^k = \sqrt{\bar{\alpha}^k} \mathbf{z}^0 + \sqrt{1 - \bar{\alpha}^k} \epsilon^k$, and the model is optimized to predict the added noise ϵ^k , resulting in a simplified loss function:

$$\mathcal{L}_{\text{diff}} = \|\epsilon^k - \epsilon_\theta(\mathbf{z}^k, k)\|^2. \quad (3)$$

In the inference phase, we can generate \mathbf{z}^0 by starting from a sample \mathbf{z}^K drawn from a standard Gaussian distribution, and the model iteratively computes \mathbf{z}^{k-1} from \mathbf{z}^k :

$$\mathbf{z}^{k-1} = \frac{1}{\sqrt{\alpha^k}} \left(\mathbf{z}^k - \frac{1 - \alpha^k}{\sqrt{1 - \bar{\alpha}^k}} \epsilon_\theta(\mathbf{z}^k, t) \right) + \sigma^k \epsilon \quad (4)$$

where $\varepsilon \sim \mathcal{N}(0, \mathbf{I})$ and σ^k is an appropriately chosen noise scale. In practice, we can accelerate the generation process by setting $\sigma^k = 0$ and use a sub-sequence of $[1, \dots, K]$ to reduce the forward steps [71].

3.2. Dynamics Prediction

Different from end-to-end world models, FlowDreamer applies a dynamics prediction module to explicitly predict the transition between consecutive frames. In robot manipulation tasks, we hope to find an intermediate representation as auxiliary information to depict the dynamics of the robot and objects. Innovated by [43, 90, 91], we choose 3D scene flow as the intermediate representation, which is general and versatile and can be collected by various flow estimation networks. In point clouds, scene flow is generally defined by the displacement of point coordinates. We can easily project an RGB-D image into point cloud space with camera intrinsics, where 2D pixels in the image with shape (H, W) are converted to $H \times W$ points in 3D space. We denote K as the camera intrinsic matrix, (u, v) as the horizontal and vertical index of pixels, and D as the depth map. Then, the pixel coordinates in camera coordinate space (x, y, z) can be calculated by:

$$\begin{bmatrix} x \\ y \\ z \end{bmatrix} = D(u, v) \cdot K^{-1} \begin{bmatrix} u \\ v \\ 1 \end{bmatrix}. \quad (5)$$

Assume the point in 3D space has a coordinate (x, y, z) at timestep t and (x', y', z') at timestep $t + 1$, the 3D scene flow is defined as follows:

$$f_{t \rightarrow t+1} = (x' - x, y' - y, z' - z). \quad (6)$$

As pixels at the same index between consecutive frames do not always represent the same 3D point, the vital challenge to get the scene flow is to find the correspondence between frames. For simulation data, we directly obtain the scene flow from the simulator backend according to the rigid transformations of every object. For real-world data, we can apply an off-the-shelf 3D scene flow estimator named RAFT-3D [76] to estimate the scene flow. If the real-world data has no depth information, we can estimate the depth by a pretrained video depth estimator [12]. The detailed scene flow obtainment pipeline are introduced in Appendix B.

We apply a dynamics prediction module to predict the 3D scene flow from time t to $t + 1$, given the RGB-D observation (I_t, D_t) and the robot action \mathbf{a}_t . The backbone of our dynamics prediction model is a conditional U-Net [65], and the robot action is integrated with the feature map via cross-attention [86]. The loss function $\mathcal{L}_{\text{flow}}$ is defined as the mean square error (MSE) between the module output $\hat{f}_{t \rightarrow t+1}$ and the estimated scene flow $f_{t \rightarrow t+1}$:

$$\mathcal{L}_{\text{flow}} = \text{MSELoss}(\hat{f}_{t \rightarrow t+1} - f_{t \rightarrow t+1}). \quad (7)$$

3.3. Future Generation

After getting the predicted scene flow, we can further predict future observations through a generative model. We choose Latent Diffusion Models as our future generation model, as it has shown outstanding capability in image generation [19, 64]. In FlowDreamer, we fine-tune the pre-trained Stable Diffusion [64] to build our future generation module, which we denote as ϵ_θ . The input of the generation module contains the current RGB-D observation (I_t, D_t) , the robot action \mathbf{a}_t , and the predicted 3D scene flow $\hat{f}_{t \rightarrow t+1}$, and the output of the module is the next RGB observation I_{t+1} . In order to generate high-resolution observations, following previous works [63, 98], we use the pre-trained variational autoencoder in Stable Diffusion [64] to compress the RGB observation I_t into latent space \mathbf{z}_t . The module output \mathbf{z}_{t+1} is also in latent space and can be decoded to image space by the pretrained decoder. Depth map D_t and the scene flow $\hat{f}_{t \rightarrow t+1}$ are firstly downsampled to the same shape of \mathbf{z}_t by several convolutional layers, and then channel-wise concatenated with \mathbf{z}_t as the input of the diffusion model:

$$\mathbf{z}_t = \text{VAE}(I_t), \quad (8)$$

$$\mathbf{c}_t = \text{downsample}(D_t, \hat{f}_{t \rightarrow t+1}), \quad (9)$$

$$\hat{\epsilon}^k = \epsilon_\theta(\text{concat}(\mathbf{z}_{t+1}^k, \mathbf{z}_t, \mathbf{c}_t), \mathbf{a}_t, k), \quad (10)$$

where k is the diffusion step, and \mathbf{z}^k is the latent to be denoised. We do not directly predict the depth map D_{t+1} , as the decoder of the diffusion model is not specially designed for metric depths. To autoregressively imagine the future, we leverage a pre-trained depth estimation model [93] with a simple DPT [61] head to predict the metric depth D_{t+1} from I_{t+1} .

In summary, our FlowDreamer trains the dynamics prediction module and the denoising U-Net jointly, and the overall loss function is:

$$\mathcal{L}_{\text{total}} = \mathcal{L}_{\text{diff}} + \alpha \mathcal{L}_{\text{flow}}, \quad (11)$$

where $\mathcal{L}_{\text{diff}}$ and $\mathcal{L}_{\text{flow}}$ are defined in Eqn. 3 and Eqn. 7, and α is a coefficient to control the weight of the two objectives.

4. Experiments

In this section, we conduct extensive experiments in four different benchmarks to verify the performance of FlowDreamer. We aim to answer three questions:

1. Is FlowDreamer effective on video prediction compared with other RGB-D world models? (Sec. 4.1)

Table 1. **Video prediction results on the SimplerEnv RT-1 benchmark.** We categorize the metrics into three groups: semantic similarity, pixel similarity, and media quality. **Bold** numbers indicate the best results, and underlined numbers indicate the second best results.

Method	Semantic Similarity		Pixel Similarity			Media Quality	
	DINOv2 L2↓	CLIP score↑	PSNR↑	SSIM↑	LPIPS↓	FID↓	FVD↓
Vanilla	12.5936	0.8999	20.5925	0.7831	0.1304	71.8069	365.0697
MinkNet	12.1569	0.9038	20.5804	0.7942	0.1252	57.9706	325.3416
SepTrain	<u>11.4512</u>	<u>0.9131</u>	<u>21.2289</u>	<u>0.8135</u>	<u>0.1097</u>	<u>45.3967</u>	245.9106
FlowDreamer	10.9922	0.9189	21.7562	0.8196	0.0993	43.5807	<u>268.3853</u>

Table 2. **Video prediction results on the Language Table benchmark.** We categorize the metrics into three groups: semantic similarity, pixel similarity, and media quality. **Bold** numbers indicate the best results, and underlined numbers indicate the second best results.

Method	Semantic Similarity		Pixel Similarity			Media Quality	
	DINOv2 L2↓	CLIP score↑	PSNR↑	SSIM↑	LPIPS↓	FID↓	FVD↓
Vanilla	10.7294	0.9473	25.6762	0.9273	0.0627	26.6415	110.4629
MinkNet	<u>10.0136</u>	<u>0.9614</u>	25.1973	0.9228	0.0642	33.5479	88.3917
SepTrain	10.2514	0.9507	<u>25.9785</u>	<u>0.9278</u>	<u>0.0571</u>	<u>21.2822</u>	<u>87.3121</u>
Ours	9.3899	0.9688	26.8907	0.9401	0.0476	20.0259	66.9215

- Can FlowDreamer facilitate model predictive control for robot manipulation tasks? (Sec. 4.2)
- How does the predicted scene flow in FlowDreamer contribute to the future prediction? (Sec. 4.3)

4.1. Video Prediction

To evaluate the future generation performance of FlowDreamer, we conduct the video prediction experiments, which require the world model to generate a full trajectory given the first frame of the video and the action trajectory. By comparing the similarity between predicted frames and ground truth frames, we can verify the future prediction capability of world models.

Datasets. We conduct video prediction experiments on RT-1 [6] and Language Table [51] benchmarks to evaluate the methods. As the real-world data do not contain the depth information, we collect training and inference trajectories from the simulator. For RT-1 environment, we use SimplerEnv [46] as the simulator. For the Language Table environment, we use the official simulation environment. Collected trajectories are split into training, validation, and test sets without overlap. Experiments on real-world data are reported in Appendix C.

Baselines. To evaluate the performance of FlowDreamer compared to other RGB-D world models, we design three different baselines: *Vanilla*, *MinkNet*, and *SepTrain*. See detailed implementation in Appendix A.

- Vanilla* is a single-stage RGB-D diffusion model, which receives current RGB-D observations as input and predicts RGB images at the next timestep. We compare it with our FlowDreamer to measure the contribution of the

dynamics prediction module.

- MinkNet* is a two-stage world model that replaces the backbone of the dynamics prediction module from U-Net to MinkowskiNet [13], a 4D sparse convolutional network for point clouds. We compare it with our FlowDreamer to demonstrate the effectiveness of the RGB-D representation.
- SepTrain* is a two-stage world model, which trains the dynamics prediction module and the Denoising U-Net separately. We compare it with our FlowDreamer to evaluate the performance of end-to-end training.

Metrics. To evaluate the video prediction performance, we use PSNR [36], SSIM [85], LPIPS [95], FID [31], and FVD [78] as the assessment metrics, and additionally calculate the latent L2 distance extracted by DINOv2 (denoted as DINOv2 L2) and the latent cosine similarity extract by CLIP (denoted as CLIP score) to estimate the semantic similarity. PSNR measures the distance between the predicted video and the ground-truth video in the pixel space, and SSIM evaluates the structural similarity between frames. LPIPS, FID, and FVD are model-based evaluation metrics that compare frames in latent feature space. LPIPS measures the distance in different feature spaces, while FID and FVD measure the distribution disparity between generated and ground-truth images or videos. DINOv2 and CLIP are large-scale pretrained models via unsupervised learning, which could robustly extract the semantic feature from the images. We assume that DINOv2 and CLIP feature distance could reflect the environment state information more than image quality metrics.

Results. Table 1 and 2 shows the quantitative results on

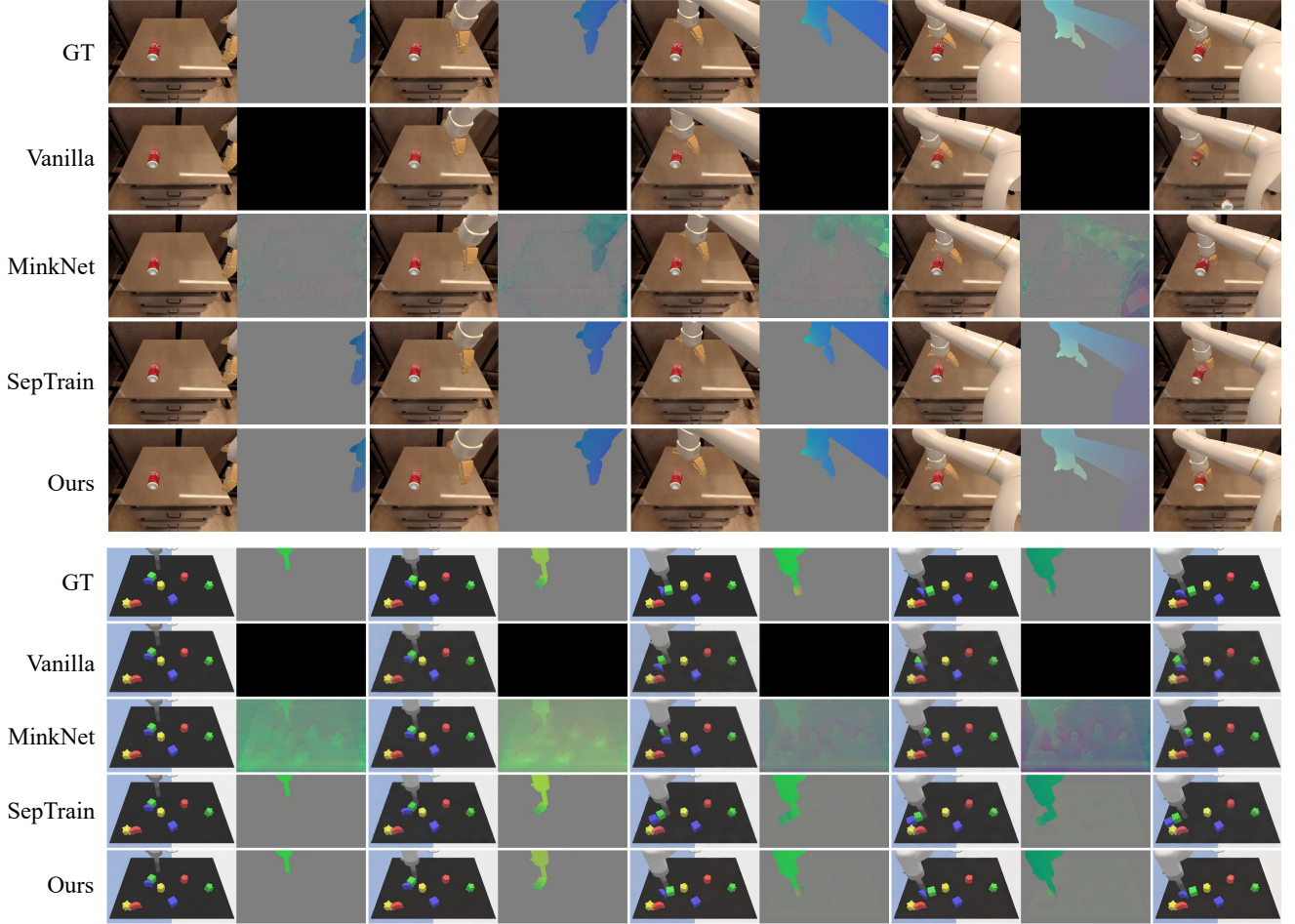


Figure 3. **Qualitative results on the SimplerEnv RT-1 and Language Table benchmark.** We show the predicted frames and the scene flows except for *Vanilla*, where only RGB frames are being predicted. The R, G, and B channel values in the flow visualization represent the components of the 3D scene flow along the x , y , and z directions, respectively, normalized by the maximum value of the scene flow.

RT-1 and Language Table benchmarks. We can observe that our FlowDreamer achieves the best performance on most of the metrics, including semantic similarity, pixel similarity, and media quality. The results demonstrate the effectiveness of our FlowDreamer. The *SepTrain* model achieves the second-best performance at most of the metrics, and the performance is very similar to our FlowDreamer. This indicates that end-to-end training is generally a better approach, while the contribution is less than that of other components. We notice that *Vanilla* and *MinkNet* have similar performances, though *MinkNet* has a similar two-stage framework and a dynamics prediction module. From the qualitative results (Fig. 3), we can see the scene flow predicted by *MinkNet* has low quality. The color of the predicted flows is similar to the ground truth flows, which shows that the direction of flows is generally correct. However, the flow predicted by *MinkNet* cannot distinguish the moving parts and the stationary parts, thus not providing efficient guidance to the downstream diffusion model. Moreover, we observe

from Fig. 3 that all predictions have a similar visual quality, but our FlowDreamer outperforms other models in environment states. This lies in the additional dynamics prediction module, which can explicitly predict the environment transition, thus resulting in more accurate future predictions.

4.2. Visual Planning

We further evaluate our FlowDreamer on visual planning tasks to show how FlowDreamer makes a difference in robot manipulation tasks. In visual planning tasks, the policy interacts with environments to minimize the difference between the observation and the goal image. For world models without any action output, model predictive control (MPC) [18, 20] methods can be applied to evaluate the performance.

Datasets. We choose VP² [77] as our visual planning benchmark. VP² is a control-centric benchmark that evaluates video prediction models by visual MPC methods. The environment contains four Robosuite [99] and seven Ro-

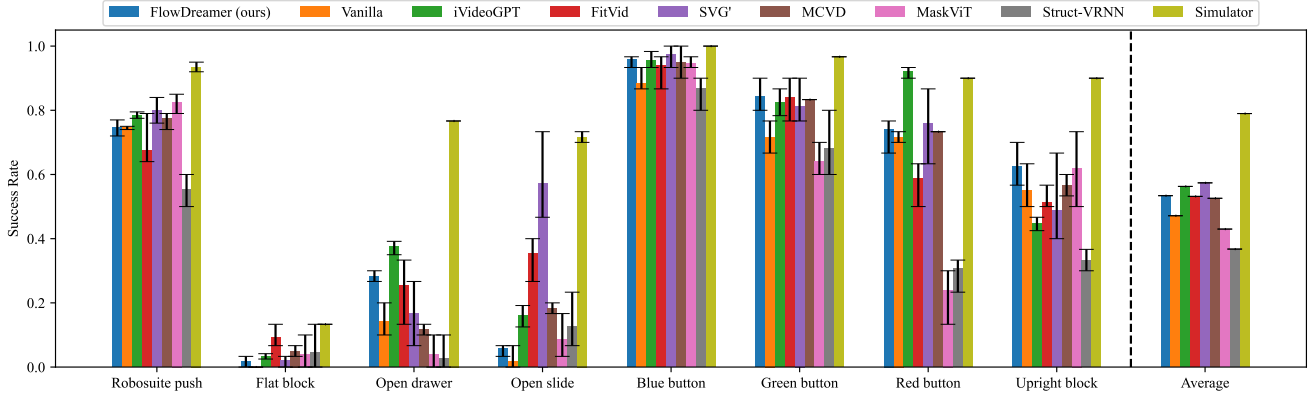


Figure 4. **Visual planning results on the VP² benchmark.** We report the mean and the min/max performance of different methods over multiple runs with different random seeds. On the right, “Average” means the average success rate over all reported tasks.



Figure 5. **Qualitative results on the Robodesk and Robosuite dataset.** The trajectory comes from the validation set, which is split from the original training trajectories and is not used for training. For our method, we show the predicted RGB images and scene flows.

boDesk [41] tasks. We run our experiments with 4 seeds on RoboDesk tasks and 3 seeds with Robosuite tasks, which keeps same with other VP² experiments.

Baselines. We compare the visual planning performance with a single-stage RGB-D diffusion world model (denoted as *Vanilla*). Moreover, following iVideoGPT [87], we choose all video generation models provided by VP² paper as our baselines, including FitVid [3], SVG' [83], MCVD [84], Struct-VRNN [55], and MaskViT [23]. We also compare our performance with iVideoGPT itself.

Metrics. Following iVideoGPT [87], we report the mini-

imum, maximum, and average success rate of our method between different random seeds. The reported baseline results are provided by previous works [77, 87], and we additionally report our performance in the same setting. For Robosuite push tasks, a cost below 0.05 is considered a success.

Results. Fig. 4 shows the visual MPC results on the VP² benchmark. From the results, we found that our FlowDreamer always performs better than the *Vanilla* model, which implies that our proposed framework works well on visual planning tasks. For other video prediction models,

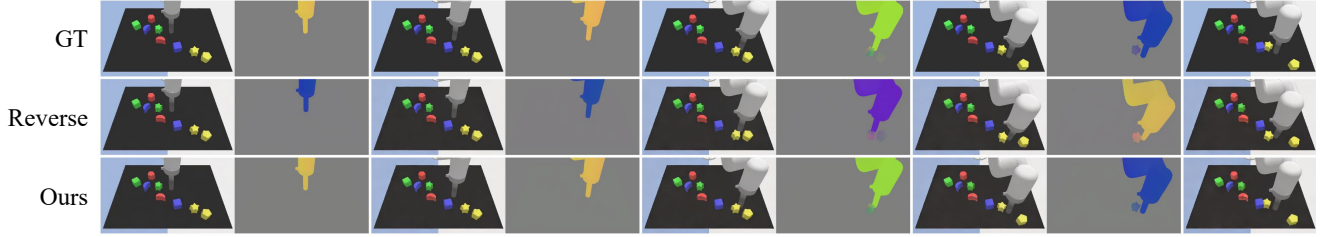


Figure 6. **The qualitative results when flows are reversed.** With reversed (therefore incorrect) scene flow, the diffusion model in FlowDreamer can only utilize action condition, leading to worse performances on future frame prediction.

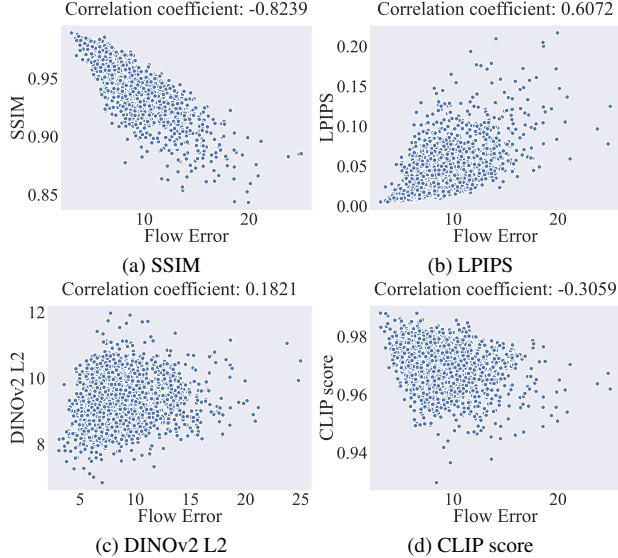


Figure 7. **The correlation between the flow prediction error and image assessment metrics.** We show the scatter plots of SSIM (higher is better), LPIPS (lower is better), DINOv2 L2 (lower is better), and CLIP score (higher is better) vs. flow error and report the correlation coefficients.

r	PSNR	SSIM	LPIPS	DINOv2	CLIP
Flow Error	-0.6704	-0.8239	0.6072	0.1821	-0.3058

Table 3. **The correlation coefficient r between the flow prediction error and image assessment metrics.** $r > 0$ indicates a positive correlation and $r < 0$ indicates a negative correlation.

FlowDreamer achieves a comparable performance on the average metric, while all video prediction baselines have a context of two frames. Our FlowDreamer performs best on some tasks, *e.g.*, Green button and Upright block, while it fails on other tasks, *e.g.*, Open slide. We hypothesize that the failure lies in that the visual reward cannot always point to the correct trajectory, which is also revealed by [87]. Fig. 5 shows the qualitative results on VP² benchmark tasks. Our model can predict the flow and the goal accurately on RoboDesk tasks, while it is hard to predict precise flow on Robosuite push tasks. We assume the reason lies in the lack

of historical context. In Robosuite tasks, objects would have velocity after being pushed by the robot arm, which cannot be reflected by a single RGB-D image. Those objects without attachment to the robot arm have scene flows, which could be misleading in prediction.

4.3. Additional Analysis on Flow Prediction

In this section, we conduct further analysis to figure out the effect of the predicted flow. We first reverse the direction of input flows at stage 2 while the robot action remains unchanged. Fig. 6 visualizes the resulting prediction. We can observe that the robot did not really take contrary actions due to the action input at stage 2, while its performance becomes worse and cannot lead to the goal state. This result shows that the scene flow predicted at stage 1 provides auxiliary information to better generate the future.

Then, we calculate the correlation between the flow prediction error and other image assessment metrics. Table 3 shows the correlation coefficient r between flow prediction error and other metrics, and Fig. 7 shows the scatter plot for SSIM, LPIPS, DINOv2 L2, and CLIP score. We notice that the flow error has a high correlation with PSNR and SSIM and a reasonable correlation with LPIPS, which demonstrates the effectiveness of the predicted flow in video prediction. For DINOv2 L2 and CLIP scores, the correlations are weak, where we infer that the semantic metrics extracted by DINOv2 and CLIP do not tell the relatively minor prediction error from the ground truth well.

5. Conclusion

We introduce FlowDreamer, an action-conditioned RGB-D world model with flow-based motion representations. FlowDreamer leverages 3D scene flow as a versatile motion representation and applies a separate dynamics prediction module to learn environment dynamics from scene flow. Despite its modularized nature, FlowDreamer can be jointly trained in an end-to-end manner. Experiments on 4 different benchmarks, including video prediction and visual planning, demonstrate the superiority of our FlowDreamer compared to other RGB-D world models. Limitations and future directions can be found in the Appendix.

References

- [1] Niket Agarwal, Arslan Ali, Maciej Bala, Yogesh Balaji, Erik Barker, Tiffany Cai, Prithvijit Chattopadhyay, Yongxin Chen, Yin Cui, Yifan Ding, et al. Cosmos world foundation model platform for physical ai. *arXiv preprint arXiv:2501.03575*, 2025. 1, 2
- [2] Eloi Alonso, Adam Jelley, Vincent Micheli, Anssi Kanervisto, Amos Storkey, Tim Pearce, and François Fleuret. Diffusion for world modeling: Visual details matter in atari. In *Advances in Neural Information Processing Systems (NeurIPS)*, 2024. 1, 2
- [3] Mohammad Babaeizadeh, Mohammad Taghi Saffar, Suraj Nair, Sergey Levine, Chelsea Finn, and Dumitru Erhan. Fitvid: Overfitting in pixel-level video prediction. *arXiv preprint arXiv:2106.13195*, 2021. 7
- [4] Kevin Black, Mitsuhiko Nakamoto, Pranav Atreya, Homer Rich Walke, Chelsea Finn, Aviral Kumar, and Sergey Levine. Zero-shot robotic manipulation with pre-trained image-editing diffusion models. In *International Conference on Learning Representations (ICLR)*, 2024. 2
- [5] Michael J Black and Padmanabhan Anandan. A framework for the robust estimation of optical flow. In *International Conference on Computer Vision (ICCV)*, 1993. 3
- [6] Anthony Brohan, Noah Brown, Justice Carbajal, Yevgen Chebotar, Joseph Dabis, Chelsea Finn, Keerthana Gopalakrishnan, Karol Hausman, Alex Herzog, Jasmine Hsu, et al. Rt-1: Robotics transformer for real-world control at scale. *arXiv preprint arXiv:2212.06817*, 2022. 2, 5, 13
- [7] Tim Brooks, Bill Peebles, Connor Holmes, Will DePue, Yufei Guo, Li Jing, David Schnurr, Joe Taylor, Troy Luhman, Eric Luhman, Clarence Ng, Ricky Wang, and Aditya Ramesh. Video generation models as world simulators, 2024. 1
- [8] Jake Bruce, Michael D Dennis, Ashley Edwards, Jack Parker-Holder, Yuge Shi, Edward Hughes, Matthew Lai, Aditi Mavalankar, Richie Steigerwald, Chris Apps, et al. Genie: Generative interactive environments. In *International Conference on Machine Learning (ICML)*, 2024. 2
- [9] Andrés Bruhn, Joachim Weickert, and Christoph Schnörr. Lucas/kanade meets horn/schunck: Combining local and global optic flow methods. *International Journal of Computer Vision (IJCV)*, 2005. 3
- [10] Arunkumar Byravan and Dieter Fox. Se3-nets: Learning rigid body motion using deep neural networks. In *International Conference on Robotics and Automation (ICRA)*, 2017. 2
- [11] Chi-Lam Cheang, Guangzeng Chen, Ya Jing, Tao Kong, Hang Li, Yifeng Li, Yuxiao Liu, Hongtao Wu, Jiafeng Xu, Yichu Yang, et al. Gr-2: A generative video-language-action model with web-scale knowledge for robot manipulation. *arXiv preprint arXiv:2410.06158*, 2024. 2
- [12] Sili Chen, Hengkai Guo, Shengnan Zhu, Feihu Zhang, Zilong Huang, Jiashi Feng, and Bingyi Kang. Video depth anything: Consistent depth estimation for super-long videos. *arXiv preprint arXiv:2501.12375*, 2025. 4, 14
- [13] Christopher Choy, JunYoung Gwak, and Silvio Savarese. 4d spatio-temporal convnets: Minkowski convolutional neural networks. In *The IEEE/CVF Conference on Computer Vision and Pattern Recognition (CVPR)*, 2019. 5, 13
- [14] Tianyuan Dai, Josiah Wong, Yunfan Jiang, Chen Wang, Cem Gokmen, Ruohan Zhang, Jiajun Wu, and Li Fei-Fei. Automated creation of digital cousins for robust policy learning. *arXiv preprint arXiv:2410.07408*, 2024. 1
- [15] Alexey Dosovitskiy, Philipp Fischer, Eddy Ilg, Philip Hausser, Caner Hazirbas, Vladimir Golkov, Patrick Van Der Smagt, Daniel Cremers, and Thomas Brox. FlowNet: Learning optical flow with convolutional networks. In *International Conference on Computer Vision (ICCV)*, 2015. 3
- [16] Yilun Du, Sherry Yang, Bo Dai, Hanjun Dai, Ofir Nachum, Josh Tenenbaum, Dale Schuurmans, and Pieter Abbeel. Learning universal policies via text-guided video generation. In *Advances in Neural Information Processing Systems (NeurIPS)*, 2024. 2
- [17] Yilun Du, Sherry Yang, Pete Florence, Fei Xia, Ayzaan Wahid, Pierre Sermanet, Tianhe Yu, Pieter Abbeel, Joshua B Tenenbaum, Leslie Pack Kaelbling, et al. Video language planning. In *International Conference on Learning Representations (ICLR)*, 2024. 2
- [18] Frederik Ebert, Chelsea Finn, Sudeep Dasari, Annie Xie, Alex Lee, and Sergey Levine. Visual foresight: Model-based deep reinforcement learning for vision-based robotic control. *arXiv preprint arXiv:1812.00568*, 2018. 1, 2, 6
- [19] Patrick Esser, Sumith Kulal, Andreas Blattmann, Rahim Entezari, Jonas Müller, Harry Saini, Yam Levi, Dominik Lorenz, Axel Sauer, Frederic Boesel, et al. Scaling rectified flow transformers for high-resolution image synthesis. In *International Conference on Machine Learning (ICML)*, 2024. 1, 4
- [20] Chelsea Finn and Sergey Levine. Deep visual foresight for planning robot motion. In *International Conference on Robotics and Automation (ICRA)*, 2017. 2, 6
- [21] Chelsea Finn, Ian Goodfellow, and Sergey Levine. Unsupervised learning for physical interaction through video prediction. In *Advances in Neural Information Processing Systems (NeurIPS)*, 2016. 2
- [22] Daniel Geng, Charles Herrmann, Junhwa Hur, Forrester Cole, Serena Zhang, Tobias Pfaff, Tatiana Lopez-Guevara, Carl Doersch, Yusuf Aytar, Michael Rubinstein, et al. Motion prompting: Controlling video generation with motion trajectories. *arXiv preprint arXiv:2412.02700*, 2024. 2
- [23] Agrim Gupta, Stephen Tian, Yunzhi Zhang, Jiajun Wu, Roberto Martín-Martín, and Li Fei-Fei. Maskvit: Masked visual pre-training for video prediction. In *International Conference on Learning Representations (ICLR)*, 2023. 7
- [24] David Ha and Jürgen Schmidhuber. Recurrent world models facilitate policy evolution. In *Advances in Neural Information Processing Systems (NeurIPS)*, 2018. 1, 2
- [25] Danijar Hafner, Timothy Lillicrap, Jimmy Ba, and Mohammad Norouzi. Dream to control: Learning behaviors by latent imagination. In *International Conference on Learning Representations (ICLR)*, 2020. 1, 2
- [26] Danijar Hafner, Timothy P Lillicrap, Mohammad Norouzi, and Jimmy Ba. Mastering atari with discrete world models. In *International Conference on Learning Representations (ICLR)*, 2021.

- [27] Danijar Hafner, Jurgis Pasukonis, Jimmy Ba, and Timothy Lillicrap. Mastering diverse domains through world models. *arXiv preprint arXiv:2301.04104*, 2023. 1, 2
- [28] Nicklas Hansen, Hao Su, and Xiaolong Wang. Td-mpc2: Scalable, robust world models for continuous control. *arXiv preprint arXiv:2310.16828*, 2023. 2
- [29] Nmenicklas A Hansen, Hao Su, and Xiaolong Wang. Temporal difference learning for model predictive control. In *International Conference on Machine Learning (ICML)*, 2022. 1, 2
- [30] Zekun Hao, Xun Huang, and Serge Belongie. Controllable video generation with sparse trajectories. In *The IEEE/CVF Conference on Computer Vision and Pattern Recognition (CVPR)*, 2018. 2
- [31] Martin Heusel, Hubert Ramsauer, Thomas Unterthiner, Bernhard Nessler, and Sepp Hochreiter. Gans trained by a two time-scale update rule converge to a local nash equilibrium. In *Advances in Neural Information Processing Systems (NeurIPS)*, 2017. 5
- [32] Jonathan Ho, Ajay Jain, and Pieter Abbeel. Denoising diffusion probabilistic models. In *Advances in Neural Information Processing Systems (NeurIPS)*, 2020. 1, 2, 3
- [33] Berthold KP Horn and Brian G Schunck. Determining optical flow. *Artificial intelligence*, 1981. 3
- [34] Siyuan Huang, Liliang Chen, Pengfei Zhou, Shengcong Chen, Zhengkai Jiang, Yue Hu, Peng Gao, Hongsheng Li, Maoqing Yao, and Guanghui Ren. Enerverse: Envisioning embodied future space for robotics manipulation. *arXiv preprint arXiv:2501.01895*, 2025. 2
- [35] Zhaoyang Huang, Xiaoyu Shi, Chao Zhang, Qiang Wang, Ka Chun Cheung, Hongwei Qin, Jifeng Dai, and Hongsheng Li. Flowformer: A transformer architecture for optical flow. In *European Conference on Computer Vision (ECCV)*, 2022. 3
- [36] Quan Huynh-Thu and Mohammed Ghanbari. Scope of validity of psnr in image/video quality assessment. *Electronics letters*, 2008. 5
- [37] Zhenyu Jiang, Cheng-Chun Hsu, and Yuke Zhu. Ditto: Building digital twins of articulated objects from interaction. In *The IEEE/CVF Conference on Computer Vision and Pattern Recognition (CVPR)*, pages 5616–5626, 2022. 1
- [38] Philipp Jund, Chris Sweeney, Nichola Abdo, Zhifeng Chen, and Jonathon Shlens. Scalable scene flow from point clouds in the real world. *IEEE Robotics and Automation Letters (RA-L)*, 2021. 3
- [39] Łukasz Kaiser, Mohammad Babaeizadeh, Piotr Miłoś, Błażej Osioński, Roy H Campbell, Konrad Czechowski, Dumitru Erhan, Chelsea Finn, Piotr Kozakowski, Sergey Levine, et al. Model based reinforcement learning for atari. In *International Conference on Learning Representations (ICLR)*, 2020. 1, 2
- [40] Anssi Kanervisto, Dave Bignell, Linda Yilin Wen, Martin Grayson, Raluca Georgescu, Sergio Valcarcel Macua, Shan Zheng Tan, Tabish Rashid, Tim Pearce, Yuhao Cao, Abdelhak Lemkhenter, Chentian Jiang, Gavin Costello, Gunshi Gupta, Marko Tot, Shu Ishida, Tarun Gupta, Udit Arora, Ryan W. White, Sam Devlin, Cecily Morrison, and Katja Hofmann. World and human action models towards gameplay ideation. *Nature*, 2025. 1, 2
- [41] Harini Kannan, Danijar Hafner, Chelsea Finn, and Dumitru Erhan. Robodesk: A multi-task reinforcement learning benchmark, 2021. 2, 7
- [42] Ishan Khatri, Kyle Vedder, Neehar Peri, Deva Ramanan, and James Hays. I can’t believe it’s not scene flow! In *European Conference on Computer Vision (ECCV)*, 2024. 3
- [43] Po-Chen Ko, Jiayuan Mao, Yilun Du, Shao-Hua Sun, and Joshua B Tenenbaum. Learning to act from actionless videos through dense correspondences. In *International Conference on Learning Representations (ICLR)*, 2023. 2, 3, 4
- [44] Guillaume Le Moing, Jean Ponce, and Cordelia Schmid. Dense optical tracking: connecting the dots. In *The IEEE/CVF Conference on Computer Vision and Pattern Recognition (CVPR)*, 2024. 3
- [45] Qixiu Li, Yaobo Liang, Zeyu Wang, Lin Luo, Xi Chen, Mozheng Liao, Fangyun Wei, Yu Deng, Sicheng Xu, Yizhong Zhang, et al. Cogact: A foundational vision-language-action model for synergizing cognition and action in robotic manipulation. *arXiv preprint arXiv:2411.19650*, 2024. 13
- [46] Xuanlin Li, Kyle Hsu, Jiayuan Gu, Karl Pertsch, Oier Mees, Homer Rich Walke, Chuyuan Fu, Ishikaa Lunawat, Isabel Sieh, Sean Kirmani, et al. Evaluating real-world robot manipulation policies in simulation. *arXiv preprint arXiv:2405.05941*, 2024. 5, 13
- [47] Jessy Lin, Yuqing Du, Olivia Watkins, Danijar Hafner, Pieter Abbeel, Dan Klein, and Anca Dragan. Learning to model the world with language. In *International Conference on Machine Learning (ICML)*, 2024. 2
- [48] Yancong Lin and Holger Caesar. Icp-flow: Lidar scene flow estimation with icp. In *The IEEE/CVF Conference on Computer Vision and Pattern Recognition (CVPR)*, 2024. 3
- [49] Xingyu Liu, Charles R Qi, and Leonidas J Guibas. FlowNet3d: Learning scene flow in 3d point clouds. In *The IEEE/CVF Conference on Computer Vision and Pattern Recognition (CVPR)*, 2019. 3
- [50] Bruce D Lucas and Takeo Kanade. An iterative image registration technique with an application to stereo vision. In *International Joint Conference on Artificial Intelligence (IJ-CAI)*, 1981. 3
- [51] Corey Lynch, Ayzaan Wahid, Jonathan Tompson, Tianli Ding, James Betker, Robert Baruch, Travis Armstrong, and Pete Florence. Interactive language: Talking to robots in real time. *IEEE Robotics and Automation Letters (RA-L)*, 2023. 2, 5
- [52] Aniruddha Mahapatra and Kuldeep Kulkarni. Controllable animation of fluid elements in still images. In *The IEEE/CVF Conference on Computer Vision and Pattern Recognition (CVPR)*, 2022. 2
- [53] Vincent Micheli, Eloi Alonso, and François Fleuret. Transformers are sample-efficient world models. In *International Conference on Learning Representations (ICLR)*, 2023. 2
- [54] Vincent Micheli, Eloi Alonso, and François Fleuret. Efficient world models with context-aware tokenization. In *International Conference on Machine Learning (ICML)*, 2024. 2

- [55] Matthias Minderer, Chen Sun, Ruben Villegas, Forrester Cole, Kevin P Murphy, and Honglak Lee. Unsupervised learning of object structure and dynamics from videos. In *Advances in Neural Information Processing Systems (NeurIPS)*, 2019. 7
- [56] Iman Nematollahi, Erick Rosete-Beas, Seyed Mahdi B Azad, Raghu Rajan, Frank Hutter, and Wolfram Burgard. T3vip: Transformation-based 3d video prediction. In *International Conference on Intelligent Robots and Systems (IROS)*, 2022. 2
- [57] Haomiao Ni, Changhao Shi, Kai Li, Sharon X Huang, and Martin Renqiang Min. Conditional image-to-video generation with latent flow diffusion models. In *The IEEE/CVF Conference on Computer Vision and Pattern Recognition (CVPR)*, 2023. 2
- [58] Junhyuk Oh, Xiaoxiao Guo, Honglak Lee, Richard L Lewis, and Satinder Singh. Action-conditional video prediction using deep networks in atari games. In *Advances in Neural Information Processing Systems (NeurIPS)*, 2015. 2
- [59] Jack Parker-Holder, Philip Ball, Jake Bruce, Vibhavari Dasagi, Kristian Holsheimer, Christos Kaplanis, Alexandre Moufarek, Guy Scully, Jeremy Shar, Jimmy Shi, Stephen Spencer, Jessica Yung, Michael Dennis, Sultan Kenjeyev, Shangbang Long, Vlad Mnih, Harris Chan, Maxime Gazeau, Bonnie Li, Fabio Pardo, Luyu Wang, Lei Zhang, Fred-eric Besse, Tim Harley, Anna Mitenkova, Jane Wang, Jeff Clune, Demis Hassabis, Raia Hadsell, Adrian Bolton, Satinder Singh, and Tim Rocktäschel. Genie 2: A large-scale foundation world model, 2024. 1, 2
- [60] Ethan Perez, Florian Strub, Harm De Vries, Vincent Dumoulin, and Aaron Courville. Film: Visual reasoning with a general conditioning layer. In *AAAI Conference on Artificial Intelligence (AAAI)*, 2018. 13
- [61] René Ranftl, Alexey Bochkovskiy, and Vladlen Koltun. Vision transformers for dense prediction. In *International Conference on Computer Vision (ICCV)*, 2021. 4
- [62] Anurag Ranjan and Michael J Black. Optical flow estimation using a spatial pyramid network. In *The IEEE/CVF Conference on Computer Vision and Pattern Recognition (CVPR)*, 2017. 3
- [63] Marc Rigter, Tarun Gupta, Agrin Hilmkil, and Chao Ma. Avid: Adapting video diffusion models to world models. *arXiv preprint arXiv:2410.12822*, 2024. 1, 2, 4
- [64] Robin Rombach, Andreas Blattmann, Dominik Lorenz, Patrick Esser, and Björn Ommer. High-resolution image synthesis with latent diffusion models. In *The IEEE/CVF Conference on Computer Vision and Pattern Recognition (CVPR)*, 2022. 1, 3, 4, 13
- [65] Olaf Ronneberger, Philipp Fischer, and Thomas Brox. U-net: Convolutional networks for biomedical image segmentation. In *Medical image computing and computer-assisted intervention (MICCAI)*, 2015. 4
- [66] Julian Schrittwieser, Ioannis Antonoglou, Thomas Hubert, Karen Simonyan, Laurent Sifre, Simon Schmitt, Arthur Guez, Edward Lockhart, Demis Hassabis, Thore Graepel, et al. Mastering atari, go, chess and shogi by planning with a learned model. *Nature*, 2020. 2
- [67] Xiaoyu Shi, Zhaoyang Huang, Weikang Bian, Dasong Li, Manyuan Zhang, Ka Chun Cheung, Simon See, Hongwei Qin, Jifeng Dai, and Hongsheng Li. Videoflow: Exploiting temporal cues for multi-frame optical flow estimation. In *International Conference on Computer Vision (ICCV)*, 2023. 3
- [68] Xiaoyu Shi, Zhaoyang Huang, Dasong Li, Manyuan Zhang, Ka Chun Cheung, Simon See, Hongwei Qin, Jifeng Dai, and Hongsheng Li. Flowformer++: Masked cost volume autoencoding for pretraining optical flow estimation. In *The IEEE/CVF Conference on Computer Vision and Pattern Recognition (CVPR)*, 2023. 3
- [69] Xiaoyu Shi, Zhaoyang Huang, Fu-Yun Wang, Weikang Bian, Dasong Li, Yi Zhang, Manyuan Zhang, Ka Chun Cheung, Simon See, Hongwei Qin, et al. Motion-i2v: Consistent and controllable image-to-video generation with explicit motion modeling. In *ACM SIGGRAPH Conference Proceedings*, 2024. 2
- [70] Jascha Sohl-Dickstein, Eric Weiss, Niru Maheswaranathan, and Surya Ganguli. Deep unsupervised learning using nonequilibrium thermodynamics. In *International Conference on Machine Learning (ICML)*, 2015. 1, 3
- [71] Jiaming Song, Chenlin Meng, and Stefano Ermon. Denoising diffusion implicit models. *arXiv preprint arXiv:2010.02502*, 2020. 1, 2, 3, 4
- [72] Deqing Sun, Xiaodong Yang, Ming-Yu Liu, and Jan Kautz. Pwc-net: Cnns for optical flow using pyramid, warping, and cost volume. In *The IEEE/CVF Conference on Computer Vision and Pattern Recognition (CVPR)*, pages 8934–8943, 2018. 3
- [73] Ruixiang Sun, Hongyu Zang, Xin Li, and Riashat Islam. Learning latent dynamic robust representations for world models. In *International Conference on Machine Learning (ICML)*, 2024. 2
- [74] Richard S Sutton. Dyna, an integrated architecture for learning, planning, and reacting. *ACM Sigart Bulletin*, 1991. 2
- [75] Zachary Teed and Jia Deng. Raft: Recurrent all-pairs field transforms for optical flow. In *European Conference on Computer Vision (ECCV)*, 2020. 3, 14
- [76] Zachary Teed and Jia Deng. Raft-3d: Scene flow using rigid-motion embeddings. In *The IEEE/CVF Conference on Computer Vision and Pattern Recognition (CVPR)*, 2021. 4, 14
- [77] Stephen Tian, Chelsea Finn, and Jiajun Wu. A control-centric benchmark for video prediction. In *International Conference on Learning Representations (ICLR)*, 2023. 2, 6, 7, 13
- [78] Thomas Unterthiner, Sjoerd Van Steenkiste, Karol Kurach, Raphael Marinier, Marcin Michalski, and Sylvain Gelly. Towards accurate generative models of video: A new metric & challenges. *arXiv preprint arXiv:1812.01717*, 2018. 5
- [79] Dani Valevski, Yaniv Leviathan, Moab Arar, and Shlomi Fruchter. Diffusion models are real-time game engines. *arXiv preprint arXiv:2408.14837*, 2024. 2
- [80] Aaron Van Den Oord, Oriol Vinyals, et al. Neural discrete representation learning. In *Advances in Neural Information Processing Systems (NeurIPS)*, 2017. 3
- [81] Kyle Vedder, Neehar Peri, Nathaniel Eliot Chodosh, Ishan Khatri, ERIC EATON, Dinesh Jayaraman, Yang Liu, Deva

- Ramanan, and James Hays. Zeroflow: Scalable scene flow via distillation. In *International Conference on Learning Representations (ICLR)*, 2024. 3
- [82] Sundar Vedula, Simon Baker, Peter Rander, Robert Collins, and Takeo Kanade. Three-dimensional scene flow. In *International Conference on Computer Vision (ICCV)*, 1999. 2, 3
- [83] Ruben Villegas, Arkanath Pathak, Harini Kannan, Dumitru Erhan, Quoc V Le, and Honglak Lee. High fidelity video prediction with large stochastic recurrent neural networks. In *Advances in Neural Information Processing Systems (NeurIPS)*, 2019. 7
- [84] Vikram Voleti, Alexia Jolicoeur-Martineau, and Chris Pal. Mcvd-masked conditional video diffusion for prediction, generation, and interpolation. In *Advances in Neural Information Processing Systems (NeurIPS)*, 2022. 7
- [85] Zhou Wang, Alan C Bovik, Hamid R Sheikh, and Eero P Simoncelli. Image quality assessment: from error visibility to structural similarity. *Transactions on Image Processing (TIP)*, 2004. 5
- [86] A Waswani, N Shazeer, N Parmar, J Uszkoreit, L Jones, A Gomez, L Kaiser, and I Polosukhin. Attention is all you need. In *Advances in Neural Information Processing Systems (NeurIPS)*, 2017. 4
- [87] Jialong Wu, Shaofeng Yin, Ningya Feng, Xu He, Dong Li, Jianye Hao, and Mingsheng Long. ivideopt: Interactive videopts are scalable world models. In *Advances in Neural Information Processing Systems (NeurIPS)*, 2024. 1, 2, 7, 8
- [88] Philipp Wu, Alejandro Escontrela, Danijar Hafner, Pieter Abbeel, and Ken Goldberg. Daydreamer: World models for physical robot learning. In *Conference on Robot Learning (CoRL)*, 2022. 2
- [89] Yuxi Xiao, Qianqian Wang, Shangzhan Zhang, Nan Xue, Sida Peng, Yujun Shen, and Xiaowei Zhou. Spatialtracker: Tracking any 2d pixels in 3d space. In *The IEEE/CVF Conference on Computer Vision and Pattern Recognition (CVPR)*, 2024. 3
- [90] Mengda Xu, Zhenjia Xu, Yinghao Xu, Cheng Chi, Gordon Wetzstein, Manuela Veloso, and Shuran Song. Flow as the cross-domain manipulation interface. In *Conference on Robot Learning (CoRL)*, 2024. 3, 4
- [91] Zhenjia Xu, Zhanpeng He, Jiajun Wu, and Shuran Song. Learning 3d dynamic scene representations for robot manipulation. In *Conference on Robot Learning (CoRL)*, 2020. 2, 4
- [92] Gengshan Yang and Deva Ramanan. Volumetric correspondence networks for optical flow. *Advances in Neural Information Processing Systems (NeurIPS)*, 32, 2019. 3
- [93] Lihe Yang, Bingyi Kang, Zilong Huang, Zhen Zhao, Xianggang Xu, Jiashi Feng, and Hengshuang Zhao. Depth anything v2. In *Advances in Neural Information Processing Systems (NeurIPS)*, 2025. 4, 14
- [94] Sherry Yang, Yilun Du, Seyed Kamyar Seyed Ghasemipour, Jonathan Tompson, Leslie Pack Kaelbling, Dale Schuurmans, and Pieter Abbeel. Learning interactive real-world simulators. In *International Conference on Learning Representations (ICLR)*, 2024. 1, 2
- [95] Richard Zhang, Phillip Isola, Alexei A Efros, Eli Shechtman, and Oliver Wang. The unreasonable effectiveness of deep features as a perceptual metric. In *The IEEE/CVF Conference on Computer Vision and Pattern Recognition (CVPR)*, 2018. 5
- [96] Haoyu Zhen, Xiaowen Qiu, Peihao Chen, Jincheng Yang, Xin Yan, Yilun Du, Yining Hong, and Chuang Gan. 3d-vla: A 3d vision-language-action generative world model. In *International Conference on Machine Learning (ICML)*, 2024. 2
- [97] Siyuan Zhou, Yilun Du, Jiaben Chen, YANDONG LI, Dityan Yeung, and Chuang Gan. Robodreamer: Learning compositional world models for robot imagination. In *International Conference on Machine Learning (ICML)*, 2024. 2
- [98] Fangqi Zhu, Hongtao Wu, Song Guo, Yuxiao Liu, Chilam Cheang, and Tao Kong. Irasim: Learning interactive real-robot action simulators. *arXiv preprint arXiv:2406.14540*, 2024. 1, 2, 4, 13
- [99] Yuke Zhu, Josiah Wong, Ajay Mandlekar, Roberto Martín-Martín, Abhishek Joshi, Soroush Nasiriany, and Yifeng Zhu. robosuite: A modular simulation framework and benchmark for robot learning. *arXiv preprint arXiv:2009.12293*, 2020. 2, 6

A. Implementation Details

Details of the dynamics prediction module. Our FlowDreamer utilizes a conditional 2D U-Net with 4 downsample and upsample layers as the dynamics prediction module. The action condition is integrated with image features via cross-attention, which is similar to Stable Diffusion. We also design a conditional MinkowskiNet [13] as a point-cloud-based baseline. The structure of the conditional MinkowskiNet is modified from MinkUNet34B in the official repository, where we replace the batch normalization layers in the basic blocks with Feature-wise Linear Modulation (FiLM) [60] layers to introduce action condition.

Training and inference details. We conduct all our experiments on an NVIDIA A800 cluster. Each model is trained on 8 GPUs in parallel, with a batch size of 16 per GPU. The denoising U-Net and the image encoder/decoder are loaded from Stable Diffusion 2.1 [64]. We only finetune the parameters of the denoising network yet freeze the weight of the encoder and decoder. All models are trained for 60k steps with a constant learning rate of $1e-4$. We use AdamW optimizer for training, and we use a mixed precision with FP16 and FP32 supported by Pytorch-Lightning. For diffusion models, we utilize a PNDM scheduler with 20 sampling steps during inference. We notice that increasing sampling steps more than 20 cannot improve the accuracy of future prediction yet is more time-consuming. The output resolution is relevant to the dataset, which will be reported in the next section.

B. Data Collection

In the main paper, we conduct experiments on 4 different simulation environments. To train world models on these environments, we need to collect feasible trajectories and calculate the ground truth 3D scene flow. Also, we conduct experiments on RT-1 real dataset, where we estimate the depth and the scene flow through depth estimators and flow estimators. Table 4 shows the dataset statistics in detail. This section will introduce the data collection pipeline.

Dataset	Resolution	Episode	Sample
RT-1 SimplerEnv	320×256	25,000	758,015
Language Table	512×288	36,000	1,447,805
RoboDesk	320×320	35,000	1,190,000
Robosuite	256×256	50,000	1,749,825
RT-1 Real	320×256	86,403	3,638,016

Table 4. **Dataset statistics.** An “episode” refers to a complete trajectory where the robot completes a task. A “sample” refers to a frame pair at timestep t and $t + 1$ with a robot action \mathbf{a}_t .

Trajectory collection. For the RT-1 SimplerEnv environment, we choose 5 tasks implemented by Sim-

plerEnv [46]: *pick_coke_can*, *pick_object*, *move_near*, *open_drawer*, *close_drawer*, and generate 5k trajectories for each task. The action trajectory is generated by CogACT [45], a foundational vision-language-action model. We only sample successful trajectories and discard failed trajectories. For the Language Table environment, we generate trajectories by the RRT* oracle policy provided in the official repositories. The task instruction format is “*push {block A} to {block B}*”. For RoboDesk and Robosuite tasks, we use the trajectories provided by VP² benchmark [77]. We load the provided initial states and actions into the simulator to collect RGB-D and flow information. Note that the observation of RoboDesk is a resized and cropped image from the original observation, which would affect the flow calculation. Our world model trains and predicts based on the original observation and crops the predicted observation to calculate the visual planning reward. The RT-1 real-world dataset is provided by the original paper [6], and we choose the preprocessed version by IRASim [98].

Scene flow obtainment. For all simulation environments, we can extract the ground truth scene flow from the simulator. Specifically, all objects in the simulator are rigid bodies or articulated objects, whose *pose* at each timestep t could be represented by a 4×4 homogeneous transformation matrix T_t . Therefore, we can calculate the position of a point at timestep $t + 1$, with the position at timestep t and the corresponding pose matrices:

$$\begin{pmatrix} \mathbf{x}_{t+1} \\ 1 \end{pmatrix} = T_{t+1} T_t^{-1} \begin{pmatrix} \mathbf{x}_t \\ 1 \end{pmatrix}, \quad (12)$$

where \mathbf{x}_t and \mathbf{x}_{t+1} are 3D point coordinates at timestep t and $t + 1$. Then the scene flow can be calculated by $f_{t \rightarrow t+1} = \mathbf{x}_{t+1} - \mathbf{x}_t$.

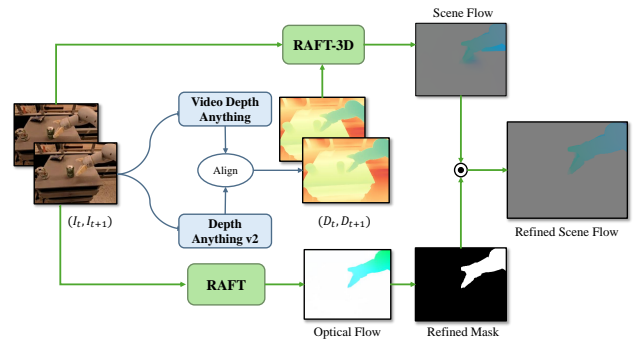


Figure 8. **Scene flow obtainment pipeline on the real-world dataset.** The consistent metric depth is estimated by Video Depth Anything and Depth Anything v2, and the 3D scene flow is estimated by RAFT-3D and refined by RAFT.

For RT-1 real world datasets, as there is no ground truth depth or pose matrix, we apply some depth estima-

Table 5. **Video prediction results on RT-1 real-world dataset.** We categorize the metrics into three groups: semantic similarity, pixel similarity, and media quality. **Bold** numbers indicate the best results.

Method	Semantic Similarity		Pixel Similarity			Media Quality	
	DINOv2 L2↓	CLIP score↑	PSNR↑	SSIM↑	LPIPS↓	FID↓	FVD↓
Vanilla	15.6659	0.8618	17.9724	0.5401	0.1882	13.1636	195.3965
Ours	15.5710	0.8687	18.6574	0.5532	0.1764	10.4547	191.3314

tion model: Depth Anything v2 [93] and Video Depth Anything [12] to estimate the metric depth, and utilize some flow estimation model: RAFT [75] and RAFT-3D [76] to estimate the 3D scene flow. The pipeline is illustrated in Fig. 8. Specifically, we first obtain the relative depths using Video Depth Anything, which can produce spatially and temporally coherent depths across frames. To get metric depths, we utilize Depth Anything V2 to estimate the metric depths and align the two depth maps by computing scale and shift parameters. Next, we input the aligned metric depth along with the RGB image into RAFT-3D to obtain frame-paired 3D scene flows and use the estimation result of RAFT to refine the scene flow by producing a flow mask.

C. Extended Experimental Results

In this section, we conduct real-world experiments to evaluate the feasibility of our pipeline. We conduct video prediction experiments on the real-world RT-1 robot manipulation dataset. The RT-1 real-world dataset contains more tasks, lighting conditions, and camera positions, making it a much harder task than on the simulation data. As there is no ground truth depth or scene flow, we leverage the estimation results as the training target. We compare FlowDreamer with the single-stage *Vanilla* world model.

Table 5 shows the performance of video prediction. FlowDreamer still performs better than *Vanilla*, while the discrepancy becomes lower than simulation data. From the qualitative examples (see Fig. 9), we could see that the ground truth scene flows estimated by RAFT-3D are not accurate, which would introduce noise into the training target. Our FlowDreamer is affected by inaccurate supervision and produces inaccurate flow predictions. However, our performance still outperforms *Vanilla*, as *Vanilla* cannot even keep the consistency of the background during generation.

D. Limitations and Future Works

While FlowDreamer has made progress, there are some limitations that could be improved by future works. First, our training data mainly come from simulation, as most of the robotic data are monocular RGB videos. Next, we did not consider any context or history in FlowDreamer, though adding more context does not conflict with our methodology. We provide a simple version of FlowDreamer that

only relies on current observations and actions, just aiming to demonstrate the effectiveness of explicit dynamics modeling. Finally, the inference of the diffusion model is relatively slow due to the progressive denoising framework, while diffusion models could achieve outstanding visual performance. Future works could explore a better tradeoff between inference time and prediction performance.



Figure 9. **Qualitative results on the RT-1 real world dataset.** The depth is estimated by Depth Anything v2, and the flow in “GT” are estimated by RAFT-3D, making it a harder scenario.